Using ADMIRE to improve minimum variance performance in the presence of reverberation clutter

Schlunk, Siegfried, Byram, Brett

Siegfried Schlunk, Brett Byram, "Using ADMIRE to improve minimum variance performance in the presence of reverberation clutter," Proc. SPIE 11602, Medical Imaging 2021: Ultrasonic Imaging and Tomography, 116020Q (15 February 2021); doi: 10.1117/12.2583314

SPIE.

Event: SPIE Medical Imaging, 2021, Online Only

Using ADMIRE to Improve Minimum Variance Performance in the Presence of Reverberation Clutter

Siegfried Schlunk[a] and Brett Byram[a]

[a]Department of Biomedical Engineering, Vanderbilt University, Nashville, TN, USA

ABSTRACT

Reverberation clutter is a difficult source of image degradation in patients, and minimum variance (MV) in particular is poorly equipped to handle such sources, as we demonstrate here. We propose that a pre-processing step such as ADMIRE should be implemented in cases with high reverberation clutter when we still want to be able to implement MV to realize improvements in lateral resolution. The ADMIRE, or aperture domain model image reconstruction, method is specifically designed to suppress or eliminate reverberant and off-axis sources of clutter while returning the decluttered channel data with its original dimensionality, allowing us to sequentially process the data with MV. We show that in simulated data this combined method results in clear improvements to image quality, contrast ratio, and target boundary thickness compared to DAS and MV alone. In *in vivo* cases, contrast ratio and general image quality are improved, and boundary thickness is generally on par with DAS and MV.

Keywords: minimum variance, reverberation clutter, ADMIRE

1. INTRODUCTION

Recent decades have experienced an increase in obesity rates in the United States.[1–3] Obese patients naturally have thicker fat layers which increase the amount of multipath scattering, or reverberation clutter, which can lead to substantial image degradation.[4] This means that reverberation clutter can be an important source of image noise that we have to contend with in *in vivo* imaging applications. Additionally, targets in obese patients may require increased imaging depth due to the thicker layers, leading to a greater desire for methods that can improve imaging quality and metrics.

One such option could be minimum variance (MV), which is a beamforming method that has demonstrated an ability to reduce and suppress off-axis sidelobe signals resulting in improved lateral resolution.[5,6] It does this by attempting to place nulls in the adaptive weights at the locations of these off-axis signals. However, in the case of similarly positioned reverberation clutter, MV is not able to improve the image quality to the same extent. Therefore we propose that a pre-processing step should be applied to reduce or eliminate reverberation clutter before the MV beamformer is applied. Specifically, we demonstrate our aperture domain model image reconstruction (ADMIRE) method's ability to reduce both reverberation and off-axis clutter prior to MV processing, creating a better image than just MV alone. We test this combined method on a variety of simple and more complex simulated cases, as well as some *in vivo* cases with reverberation clutter.

2. METHODS

2.1 Delay-and-Sum (DAS)

Delay-and-sum (DAS) is the gold standard beamformer in part due to its low computational complexity and real-time performance. It is mathematically defined as

$$S_{\mathrm{DAS}}(x,z) = \sum_{i=1}^{M} \mathrm{w}_i(z) s_i(x,z), \tag{1}$$

Further author information: (Send correspondence to S.S.)
S.S.: E-mail: siegfried.g.schlunk@vanderbilt.edu
B.B.: E-mail: brett.c.byram@vanderbilt.edu

Medical Imaging 2021: Ultrasonic Imaging and Tomography, edited by Brett C. Byram, Nicole V. Ruiter, Proc. of SPIE Vol. 11602, 116020Q · © 2021 SPIE
CCC code: 1605-7422/21/$21 · doi: 10.1117/12.2583314

where x is the lateral position, z is a discrete time index, M is the total number of channels, $\mathrm{w}_i(z)$ is the weighting factor for channel i, and $s_i(x,z)$ is the delayed channel data. DAS can be further tuned by adjusting the weighting factor, such as with Hamming or Hanning apodization to reduce sidelobes.[7]

2.2 Minimum Variance (MV)

Minimum variance (MV) can be thought of as an adaptively weighted DAS image where the weighting factor is optimized to improve lateral resolution by reducing off-axis clutter.[5,6] The optimized weights are defined as

$$\mathbf{w} = \frac{R^{-1}\mathbf{e}}{\mathbf{e}^H R^{-1}\mathbf{e}}, \tag{2}$$

where $\mathbf{e}$ is the steering vector, H is the conjugate transpose, and R is the covariance matrix defined as

$$R(z) = \mathrm{E}[\mathbf{s}(z)\mathbf{s}(z)^H], \tag{3}$$

where $\mathrm{E}[\cdot]$ denotes the expectation and $\mathbf{s}(z)$ is the delayed aperture signal at depth z. To ensure R is invertible we use subarray averaging and diagonal loading methods.[6] Specifically, we used subarray lengths of $L = 0.5M$ as recommended and diagonal loading defined as $\epsilon = \Delta \cdot \mathrm{tr}(\hat{R})$, where $\Delta = 1/(100L)$ for improved lateral resolution. The estimated MV signal is then defined as

$$\hat{\mathbf{S}}_{\mathrm{MV}}(z) = \frac{1}{M-L+1}\sum_{l=0}^{M-L}\mathbf{w}(z)^H\bar{\mathbf{s}}(z), \tag{4}$$

where $\bar{\mathbf{s}}(z)$ is the delayed channel data for a given subarray.

2.3 Aperture Domain Model Image Reconstruction (ADMIRE)

Aperture domain model image reconstruction (ADMIRE) is a method for removing reverberation and off-axis clutter, as well as suppressing wavefront aberration. Byram et al. presented a detailed explanation of the components of the algorithm,[8] and additional information can be found elsewhere.[9,10]

Processing begins by applying dynamic receive delays to the channel data. This delayed data is then divided into multiple overlapping windows along the axial dimension, along which the Fourier transform is performed (i.e. a short-time Fourier transform (STFT)). This data can then be analyzed for each primary frequency component using a physics-based model derived from the well-defined physics of linear wave propagation. It is composed of the predicted aperture domain signals created from scatterers throughout the field-of-view of the transducer, as defined by the equation

$$p_s(x;t,\omega) = \sum_{n=0}^{N-1} A(x;x_n,z_n,\tau_n,\omega)e^{jk\tau(x;x_n,z_n,\tau_n)}, \tag{5}$$

where x is the position along the aperture, t and ω specify the time and frequency for the signal, k is the corresponding wave number, N is the total number of scatterers arriving at the transducer at time t, and $\tau(x;x_n,z_n,\tau_n)$ is the wavefront delay for a signal received from (x_n,z_n) at time τ_n. Note that τ_n can be different from t so that subtle shifts in phase can be included in the model. Finally, $A(x;x_n,z_n,\tau_n,\omega)$ is the amplitude modulation across the aperture caused by the STFT windows and element sensitivity.

These modeled signals are combined into a model matrix, X, which allow for representing a given aperture domain signal, y, by its component sources, β, by

$$y = X\beta, \tag{6}$$

where y is for a specific wave number k and location (x_n,z_n), X is the set of physical model predictors, and β the set of solved model coefficients. Fig. 1 is included to give an intuitive sense of how each signal in the model matrix X relates to a specific physical source location. In theory, solving (6) by multiplying by X^{-1} reveals the exact composition of β, which reveals the specific physical locations of the various reflected echoes that linearly combine to form y. For the current location being processed, ADMIRE then chooses some small

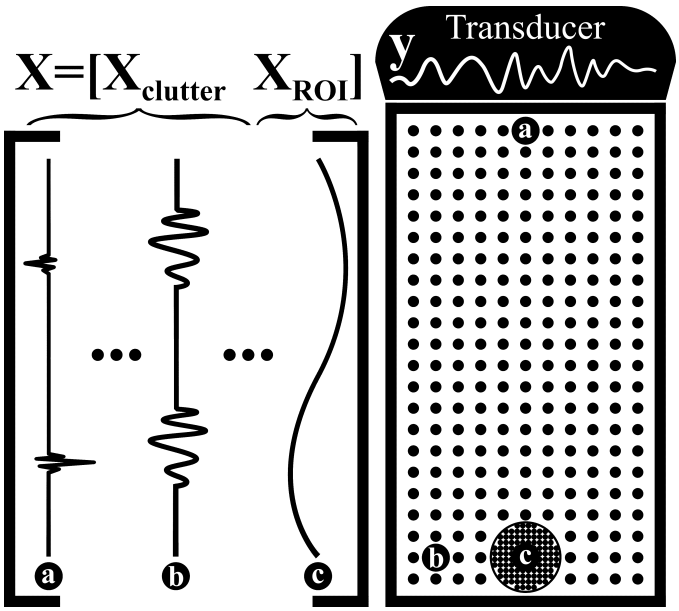

Figure 1. Example model X, composed of a set of estimated signals from locations considered to be clutter (sparsely sampled, e.g a and b), and a set from locations considered to be region of interest (highly sampled, e.g. c). For a given aperture domain signal y, the model can be used to estimate which sources are components of the received signal, thus removing the signal components that are not from the ROI.

region of interest (ROI) centered at that location and can simply remove the coefficients for sources outside of that ROI, and reconstruct the decluttered signal as

$$y_{\text{decluttered}} = X\beta_{\text{ROI}}, \tag{7}$$

using only the coefficients β_{ROI} corresponding to signals originating from inside the ROI. This removes any signals located off-axis or from reverberant sources.

In practice, (6) is ill-posed due to the relatively small size of y compared to the potentially large size of X depending on the sampling of the model space. To solve for the model predictors, ADMIRE uses the elastic-net regularization technique[11] with the optimization equation

$$\hat{\beta} = \arg\min_{\beta}(||y - X\beta||^2 + \lambda(\alpha||\beta||_1 + (1-\alpha)||\beta||_2^2/2)), \tag{8}$$

where $||\beta||_1$ is the L1 norm, $||\beta||_2$ is the L2 norm, and α is set between 0 and 1 to control the weighting between L1 and L2. λ is a regularization parameter which controls the degrees of freedom.[12] Here, we choose $\alpha = 0.9$ and $\lambda = (0.0189/10)y_{\text{RMS}}$ based on the root mean square (RMS) of the signal y.

Once the aperture domain signal has been decluttered using the coefficients solved by the elastic-net and (7), the inverse STFT is applied to return to the time domain.[13] This results in a decluttered version of the channel data that can still be processed using other beamformers, if desired, or simply combined using the delay-and-sum (DAS) equation (1). In this paper, ADMIRE results do not include any additional post-processing except with MV, where stated.

2.4 Simulated Single Target Phantoms

We used Field II[14,15] to simulate individual scatterers without any background speckle. The simulation parameters are detailed in Table 1. The primary and off-axis targets were simulated at a depth of 3 cm, while the reverberation points were simulated at a depth of 0.5 cm and then time shifted to the same time index as our primary target, similar to as done in previous work.[16,17]

Table 1. Field II Simulation Parameters for Contrast Target Phantoms

Parameter	Value
Number of elements	117
Number of mathematical elements (lateral)	7
Number of mathematical elements (elevation)	11
Element height	4 mm
Element width	0.254 mm
Kerf	0.003 mm
Lateral pitch	0.257 mm
Center frequency (f_c)	3 MHz
Sampling frequency (simulation) (f_s)	640 MHz
Sampling frequency (downsampled) (f_s)	40 MHz
Bandwidth	60%
Transmit focal depth	3 cm
Transmit/receive f-number	1

This fundamental simulation was specifically included to cleanly demonstrate how MV behaves when a primary target is receiving interference from an off-axis target versus from a reverberant target. This allowed us to more easily observe how these different targets affect the weights from MV, since we could calculate the optimized weights for each phantom and store the weights for the beam centered on the primary target. We then applied those fixed weights to all beams in a single scatterer phantom to create a high-resolution beamplot, showing the regions where MV was trying to suppress off-axis interference, which is the beam response.

2.5 Simulated Cyst Phantoms

For a more traditional simulation, we again used Field II to simulate 5 mm diameter anechoic cysts using the same parameters as in Table 1, creating six independent speckle realizations. We then simulated reverberation clutter using the method described by Byram and Shu.[16,17] We combined the reverberation clutter and cyst channel data such that it satisfied a signal-to-clutter ratio (SCR) as defined by

$$\mathrm{SCR} = 10\log_{10}\left(\frac{P_{\mathrm{SOI}}}{\alpha^2 P_{\mathrm{clutter}}}\right), \tag{9}$$

where P_{SOI} is the power of the channel data of the cyst phantom, P_{clutter} is the power of the channel data of the reverberation clutter, and α is the scalar for the reverberation clutter in order to achieve the desired SCR. The power was calculated for two regions at equivalent depths in the backgrounds of the data, and we created reverberation cases that represented 20, 10, and 0 dB SCR compared to the cyst channel data. Though there has been relatively little research into classifying what a low or high reverberation clutter case looks like in terms of SCR, we have previously determined that we believe that 0 dB SCR represents a high amount of clutter corresponding to a difficult-to-image patient, while 20 dB represents a much lower clutter case.[18] This is backed up by other studies such as one where bladder wall (signal) to clutter ratios were between 30 and 0 dB for all sources of clutter including reverberation,[19] suggesting our range of 20 to 0 dB SCR is reasonable for *in vivo* scenarios. All cases and levels of clutter where processed using MV, with and without pre-processing with ADMIRE.

2.6 *In vivo* Liver Data

We additionally captured *in vivo* liver data from patients undergoing trans-arterial chemoembolization (TACE) using a Verasonics Vantage Ultrasound System (Verasonics, Inc., Kirkland, WA) with a C52 curvilinear transducer. A center frequency of 4.1667 MHz was used to acquire 64 angles spanning 37° at a focused depth of 6 cm. Two of these cases were chosen and processed using MV, with and without pre-processing with ADMIRE.

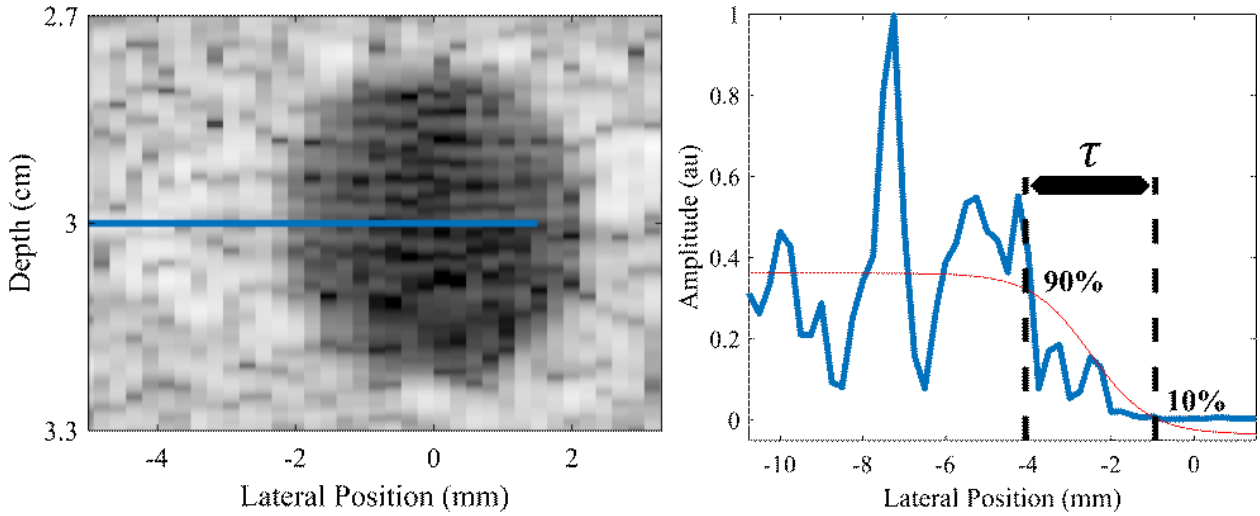

Figure 2. (Left) DAS image of a simulated anechoic cyst with no added reverberation clutter. The blue line indicates the location where the data for the sigmoid fit is taken. (Right) the enveloped data and the fit function are shown and the 10% and 90% bounds used to calculate the thickness estimate, τ are indicated.

2.7 Contrast Ratio, CNR, and Boundary Thickness

For the simulated cyst phantoms and the *in vivo* liver cases, we computed contrast ratio, contrast-to-noise ratio (CNR), and the lateral tissue boundary thickness to quantify ease of detecting tissue boundaries. Contrast ratio and CNR were defined as

$$\text{contrast ratio} = 20\log_{10}\left(\frac{\mu_{\text{ROI}}}{\mu_{\text{background}}}\right) \tag{10}$$

$$\text{CNR} = \frac{|\mu_{\text{ROI}} - \mu_{\text{background}}|}{\sqrt{\sigma^2_{\text{ROI}} + \sigma^2_{\text{background}}}}, \tag{11}$$

where μ is the mean value and σ is the standard deviation calculated from the enveloped, but not log compressed, data. Boundary thickness was defined similar to our previous work,[20] where a sigmoid function is fit to the enveloped, but not log compressed, data. We estimate the thickness as the transition length τ from 10% to 90% of the amplitude of the fit sigmoid function, as demonstrated in Fig. 2. The sigmoid function fit was defined as

$$\text{y} = \frac{a}{1 + e^{-b(\text{x}-c)}} + d, \tag{12}$$

where the parameters a, b, c, d where determined by using a custom-defined model with the fit function in MATLAB (The MathWorks, Natick, MA, USA), using the the non-linear least squares fitting procedure. For the simulated cysts, where the exact cyst boundary is known, c was fixed as that boundary location to ensure fairness between methods. For the *in vivo* cases, the parameter c was constrained within reasonable bounds based on the DAS image to prevent extreme fits. In all cases, since the sigmoid can often be fit poorly due to the random speckle pattern, outliers were removed based on being more than three scaled median absolute deviations away from the median. We computed contrast ratio, CNR, and the thickness estimate for all methods and all simulated cysts and *in vivo* cases.

3. RESULTS

Fig. 3 shows a summary of the issue. The beamplot in Fig. 3G shows the appearance of the null near the primary target in the case with an off-axis target, but the case with similarly located reverberation clutter shows the beamplot is mostly unaffected. The B-mode images show that while MV does improve the image quality in both the off-axis and reverberation cases, the reverberation clutter is relatively untouched. When ADMIRE is applied, both the off-axis and reverberation clutter are significantly reduced and the sidelobes are lowered,

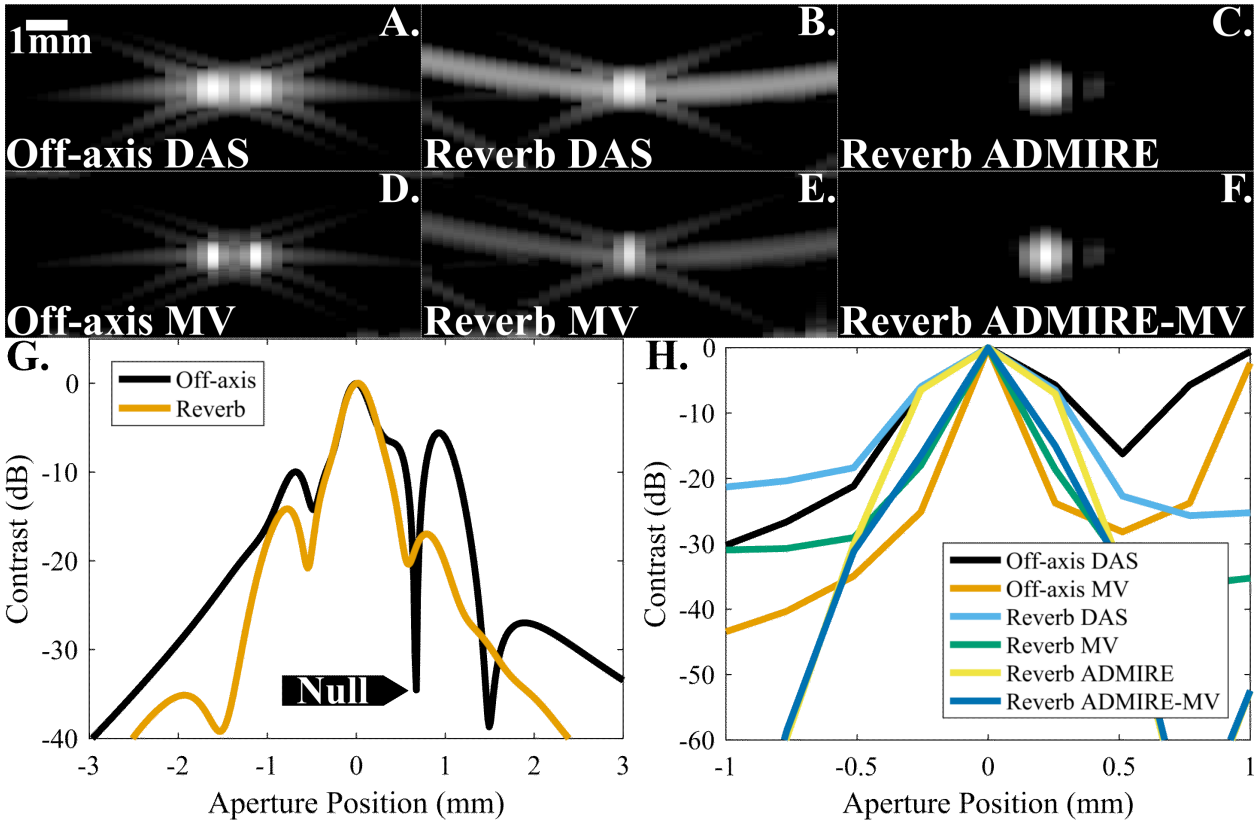

Figure 3. B-mode images with a 60 dB dynamic range of a primary target placed in the center of the aperture with an off-axis target (A,D) or reverberation clutter (B,C,E,F). (A,B) DAS images, (C) ADMIRE image, (D,E) MV images, and (F) MV image processed after ADMIRE. (G) shows the beamplot for the case with the off-axis target versus the reverberation clutter, highlighting the null in the off-axis case. (H) shows the point spread function for the images through the primary target.

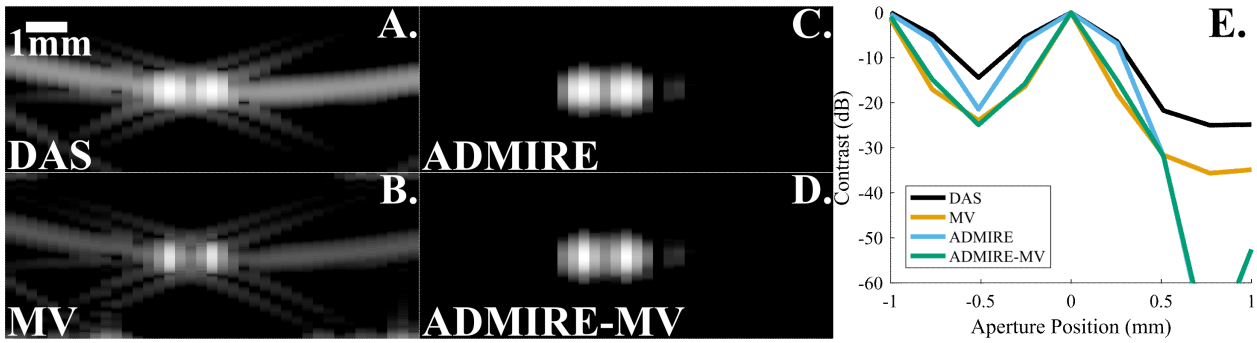

Figure 4. (A) DAS, (B) MV, (C) ADMIRE, and (D) ADMIRE-MV B-mode images with a 60 dB dynamic range of a primary target placed in the center of the aperture with an off-axis target and reverberation clutter simultaneously. (E) point spread function for the images through the primary target.

and the ADMIRE-MV case shows the improved image quality of the ADMIRE image with the improved lateral resolution of the MV image. Fig. 4 shows a combined version where the off-axis target and reverberation target are located on either side of the primary target in the same image. Here we see similar results as before, where the reverberation clutter is mostly untouched until ADMIRE is applied. The point spread function again shows that ADMIRE-MV has very similar resolution compared to MV for the primary and off-axis targets, so it would seem that the pre-processing with ADMIRE is not sacrificing MV performance.

A selection of the simulated anechoic cysts with and without added reverb is shown in Fig. 5, and the contrast

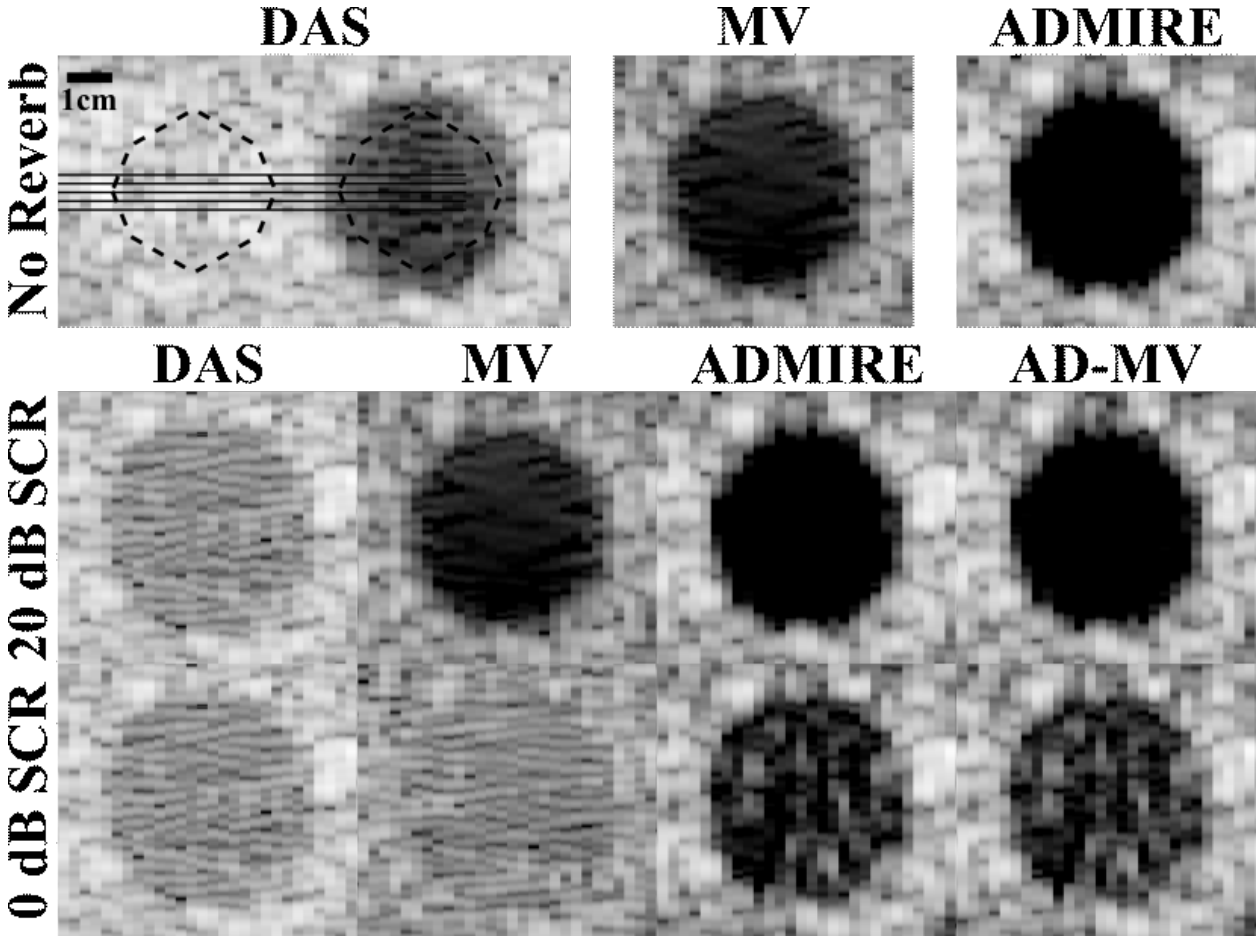

Figure 5. No reverb, 20 dB SCR (low reverb), and 0 dB SCR (high reverb) cases processed with DAS, MV, ADMIRE, and ADMIRE-MV displayed on a 60 dB dynamic range. The dashed regions indicate where the target and background areas were taken for contrast ratio and CNR measurements, and the solid black lines indicate the range of depths at which boundary thickness was estimated (performed on both the left and right sides of the cyst). Qualitatively, we see that MV performs adequately in no reverb and low reverb environments, but arguably does worse compared to DAS in the high reverb case. In comparison, the ADMIRE-MV images, where ADMIRE was used first as a pre-processing step before MV, show improvements compared to base MV for all cases.

Table 2. Contrast Ratio (dB) at Varying Levels of Added Reverberation Clutter

	Contrast Ratio (dB)			
Added Reverb (SCR)	None	20 dB (low)	10 dB	0 dB (high)
DAS	-33.1±1.4	-15.0±0.7	-15.0±0.7	-15.0±0.7
MV	-34.4±.0.6	-34.4±0.6	-34.4±0.6	-9.2±0.8
ADMIRE	-71.1±2.1	-71.1±2.1	-71.1±2.1	-32.5±3.0
ADMIRE-MV	-67.5±2.3	-67.6±2.3	-67.5±2.3	-29.3±2.3

ratio and CNR results are found in Table 2 and Table 3, respectively. In no reverb and 20 dB SCR (low reverb) cases, MV demonstrates improved apparent image quality and contrast ratio compared to DAS, though due to increased variance in the cyst region, CNR is lower. The ADMIRE-MV method shows further improvements to contrast ratio without changes to the CNR compared to MV. In the 0 dB SCR (high reverb) case, MV actually performs worse compared to DAS in terms of image quality, contrast ratio, and CNR. In comparison, MV with ADMIRE pre-processing shows a marked improvement in contrast ratio compared to both DAS and MV, and an improved CNR compared to MV.

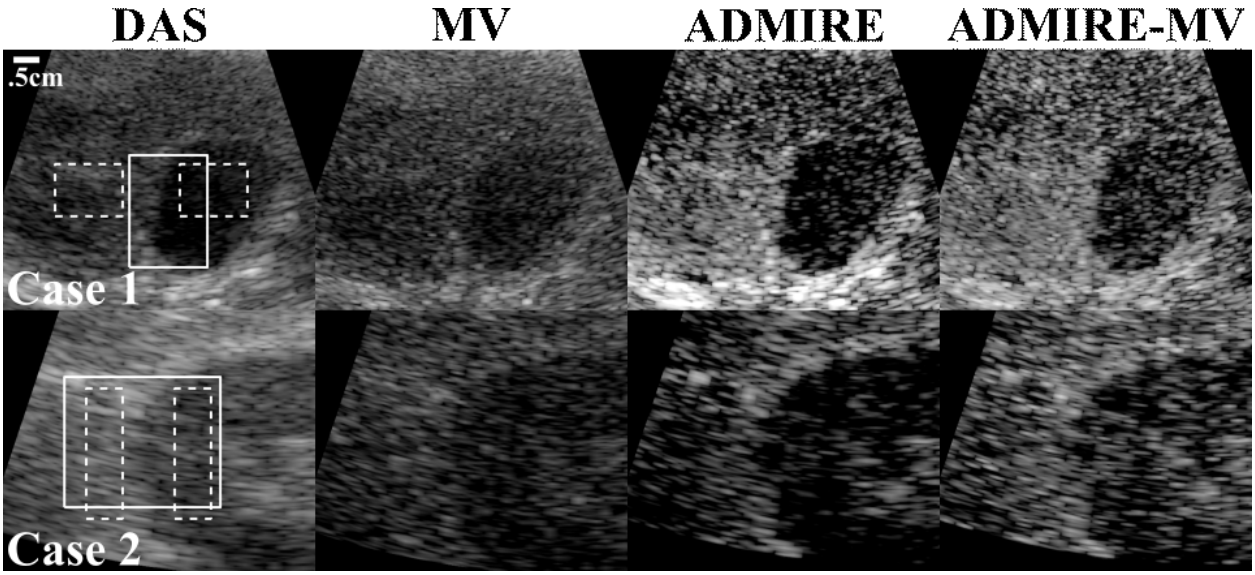

Figure 6. Two *in vivo* liver cases processed with DAS, MV, ADMIRE, and ADMIRE-MV displayed on a 60 dB dynamic range. The dashed regions indicate where the target and background areas were taken for contrast ratio and CNR measurements, and the solid regions indicate the range of depths at which boundary thickness was estimated. In both cases, the ADMIRE-MV method seems to produce images where the boundaries and the target in general are more well-defined compared to base MV.

Table 3. Contrast-to-Noise Ratio (CNR) at Varying Levels of Added Reverberation Clutter

	Contrast-to-Noise Ratio (CNR)			
Added Reverb (SCR)	None	20 dB (low)	10 dB	0 dB (high)
DAS	1.9±0.1	1.6±0.1	1.6±0.1	1.6±0.1
MV	1.5±0.1	1.5±0.1	1.5±0.1	1.0±0.1
ADMIRE	1.6±0.1	1.6±0.1	1.6±0.1	1.4±0.1
ADMIRE-MV	1.5±0.1	1.5±0.1	1.5±0.1	1.4±0.1

Table 4. Summary Statistics for *in vivo* Cases

		Contrast Ratio (dB) and CNR			
		DAS	MV	ADMIRE	ADMIRE-MV
Case 1	Contrast (dB)	-9.9	-3.5	-20.5	-14.2
	CNR	0.94	0.42	0.85	0.87
Case 2	Contrast (dB)	-9.8	-8.1	-13.1	-10.3
	CNR	0.94	0.75	0.65	0.55

The two *in vivo* cases are shown in Fig. 6, showing cases where MV produces worse images than the default DAS method. The contrast ratio and CNR are both found in Table 4, confirming that MV does struggle with these *in vivo* cases. ADMIRE shows an improved contrast ratio at the cost of CNR compared to DAS and MV, and the ADMIRE-MV combined method likewise shows improved contrast ratio compared to both DAS and MV, but again worse CNR due to increased variance of the speckle pattern. Compared to the trends in the simulated cyst data, we expect that Case 1 is probably a reasonably high reverberation case due to the substantially worse performance of MV compared to DAS, and Case 2 is likely a somewhat high reverberation case since the metrics are fairly similar to DAS. As in the simulated high reverberation case, pre-processing with ADMIRE resulted in improved contrast ratio with worse CNR compared to DAS. However, in comparison to MV, in Case 1 ADMIRE-MV has improved CNR while in Case 2 CNR is worse.

Finally, we created box plots for the estimated boundary thickness from the sigmoid function fits shown in Fig. 7 for both simulated and *in vivo* examples. After removing outliers due to imprecise or incorrect sigmoid

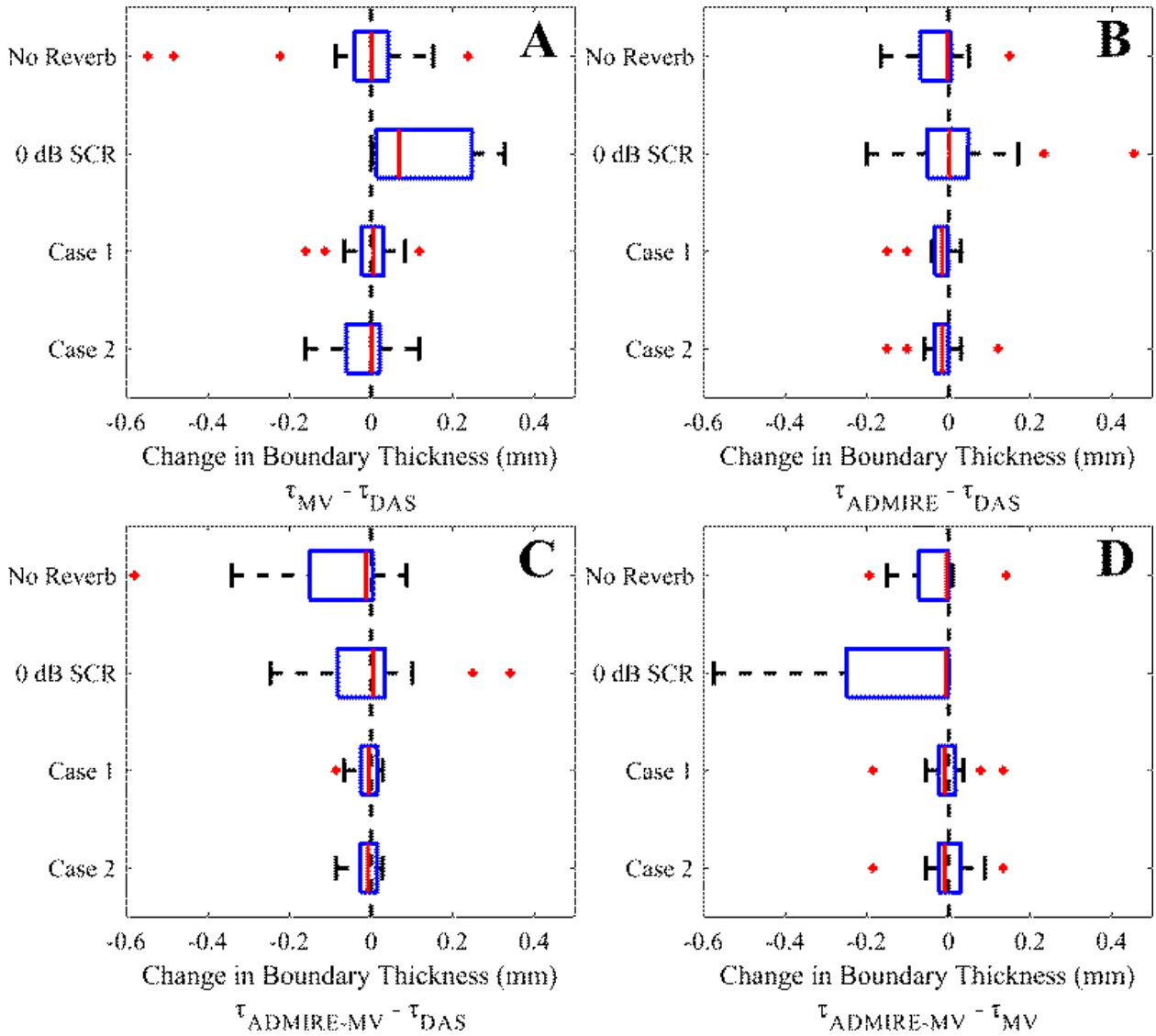

Figure 7. Box plots showing the change in boundary thickness (mm) for the simulated anechoic cysts with No Reverb, 0 dB SCR added reverberation clutter (high clutter), and the *in vivo* Case 1 and Case 2. (A) Change in thickness of MV compared to DAS. (B) Change in thickness of ADMIRE compared to DAS. (C) Change in thickness of ADMIRE-MV compared to DAS. (D) Change in thickness of ADMIRE-MV compared to MV. For all plots, the format (Method 1) - (Method 2) means that negative changes indicate Method 1 has less thickness (and therefore a more well-defined boundary) compared to Method 2, which is preferable. For example, in (A) in the 0 dB SCR case, the changes in thickness are positive, indicating that MV was worse (had less well-defined boundaries) compared to DAS.

fits, we had $n = 17$ fits for the simulated anechoic cysts, $n = 19$ fits for *in vivo* Case 1, and $n = 21$ fits for *in vivo* Case 2. Each box plot shows a particular method versus either DAS or MV as noted. Therefore, negative values indicate lower (improved) thickness, while positive values indicate a less well-defined boundary. Pairing the results this way allows us to avoid skewing the results due to some regions of the border being naturally thicker compared to others in the image.

In the simulated case with no added reverberation clutter, we see that MV and DAS perform nearly equivalently on average, with each performing better in occasional situations. However, in the 0 dB SCR (high reverb) case, MV performs exclusively worse compared to DAS. In comparison, ADMIRE-MV performs somewhat consistently better compared to DAS, and exclusively better compared to MV. The differences *in vivo* are less

significant, in particular we see that DAS, MV, and ADMIRE-MV are all performing essentially on par with each other in both *in vivo* cases.

4. DISCUSSION AND CONCLUSIONS

We have demonstrated a variety of both simulated and *in vivo* examples of how MV can struggle to perform in situations with high reverberation clutter due to its inability to handle such clutter sources. The single target simulations show precisely how MV tends to ignore reverberation clutter compared to those off-axis sources which it handles so well. Though this does not necessarily impact lateral resolution, it does impact general image quality, and in cases with especially high reverberation clutter, it may begin to impact resolution as we saw in the simulated anechoic cyst examples where boundary thickness was degraded in high reverberation cases.

As a result, we proposed that MV should be coupled with a pre-processing step in these high reverberation scenarios, where another method could first remove these difficult clutter sources prior to processing with MV. Here, we demonstrated that with ADMIRE, though in theory we expect any method that can remove reverberation clutter without reducing the dimensionality of the channel data to have similar results, for example using deep neural networks.[21] The single target simulations showed how ADMIRE can almost entirely remove reverberation clutter sources in some cases, substantially improving the general image quality of the final MV image without impacting the lateral resolution improvements of MV.

The simulated anechoic cysts further demonstrate our observations, where MV actually performs worse than normal DAS in the most extreme reverberation clutter cases, having lower contrast ratio, CNR, and worse boundary thickness of the cyst. However, pre-processing with ADMIRE to remove the reverberation clutter results in a much more well-defined cyst with improved contrast ratio and boundary thickness compared to both DAS and MV. In lower or no reverberation cases ADMIRE-MV still has improved image quality and contrast ratio compared to MV, though the boundary thickness is not significantly different.

The *in vivo* results demonstrate some examples of reverberation clutter cases where MV performs on par or worse compared to DAS based on all metrics we calculated. Case 1 is especially difficult for MV, where the resulting image makes the target substantially less well-defined compared to normal DAS, with significantly less contrast in the MV image. The boundary thickness estimates for both *in vivo* cases did not show significant differences for ADMIRE-MV versus DAS or MV, but in both cases the method did improve image contrast and general target clarity, and notably did lessen the boundary thickness variance compared to MV. This suggests that these ADMIRE-MV images still represent improvements to just MV alone, since the general image quality seems improved and the targets do appear more well-defined. We expect that the inconclusive boundary thickness tests may partially be due to the general difficulty we had getting good fits of the *in vivo* data, though we additionally hope that future parameter tuning to either the ADMIRE or MV algorithms may also be able to get us more conclusive results.

Acknowledgment

The authors would like to thank the staff of the Vanderbilt University ACCRE computing resource. This work was supported by NIH grants R01EB020040 and S10OD016216-01, and additionally by NSF award IIS-1750994.

REFERENCES

[1] Flegal, K. M., Carrol, M. D., Kuczmarski, R. J., and Johnson, C. L., "Overweight and obesity in the United States: Prevalence and trends, 1960–1994," *Int J Obes Relat Metab Disord* **22**(1), 39–47 (1998).

[2] Flegal, K. M., Carrol, M. D., Ogden, C. L., and Johnson, C. L., "Prevalence and trends in obesity among U.S. adults, 1999–2000," *JAMA* **288**(14), 1723–1727 (2002).

[3] Flegal, K. M., Carrol, M. D., Ogden, C. L., and Curtin, L. R., "Prevalence and trends in obesity among US adults, 1999–2008," *JAMA* **303**(3), 235–241 (2010).

[4] Dahl, J. J., Hyun, D., Li, Y., Jakovljevic, M., Bell, M. A. L., Long, W. J., Bottenus, N., Kakkad, V., and Trahey, G. E., "Coherence beamforming and its applications to the difficult-to-image patient," *IEEE International Ultrasonics Symposium (IUS)* (2017).

[5] Holfort, I. K., Gran, F., and Jensen, J. A., "Broadband minimum variance beamforming for ultrasound imaging," *IEEE Transactions on Ultrasonics, Ferroelectrics, and Frequency Control* **56**(2), 314–325 (2009).

[6] Synnevåg, J.-F., Austeng, A., and Holm, S., "Adaptive Beamforming Applied to Medical Ultrasound Imaging," *IEEE Transactions on Ultrasonics, Ferroelectrics, and Frequency Control* **54**(8), 1606–1613 (2007).

[7] Matrone, G., Savoia, A. S., Caliano, G., and Magenes, G., "The Delay Multiply and Sum Beamforming Algorithm in Ultrasound B-Mode Medical Imaging," *IEEE Transactions on Medical Imaging* **34**(4), 940–949 (2015).

[8] Byram, B., Dei, K., Tierney, J., and Dumont, D., "A Model and Regularization Scheme for Ultrasonic Beamforming Clutter Reduction," *IEEE Transactions on Ultrasonics, Ferroelectrics, and Frequency Control* **62**(11), 1913–1927 (2015).

[9] Dei, K. and Byram, B., "The Impact of Model-Based Clutter Suppression on Cluttered, Aberrated Wavefronts," *IEEE Transactions on Ultrasonics, Ferroelectrics, and Frequency Control* **64**(10), 1450–1464 (2017).

[10] Byram, B. and Jakovljevic, M., "Ultrasonic Multipath and Beamforming Clutter Reduction: A Chirp Model Approach," *IEEE Transactions on Ultrasonics, Ferroelectrics, and Frequency Control* **61**(3), 428–440 (2014).

[11] Zou, H. and Hastie, T., "Regularization and variable selection via the elastic net," *Journal of the Royal Statistical Society: Series B (Statistical Methodology)* **67**(2), 301–320 (2005).

[12] Tibshirani, R. J. and Taylor, J., "Degrees of Freedom in Lasso Problems," *The Annals of Statistics* **40**(2), 1198–1232 (2012).

[13] Yang, B., "A Study of Inverse Short-Time Fourier Transform," *IEEE International Conference on Acoustics, Speech and Signal Processing* , 3541–3544 (2008).

[14] Jensen, J. A., "Field: A Program for Simulating Ultrasound Systems," *Paper presented at the 10th Nordic-Baltic Conference on Biomedical Imaging Published in Medical & Biological Engineering and Computing* **34**, 351–353 (1996).

[15] Jensen, J. A. and Svendsen, N. B., "Calculation of Pressure Fields from Arbitrarily Shaped, Apodized, and Excited Ultrasound Transducers," *IEEE Transactions on Ultrasonics, Ferroelectrics, and Frequency Control* **39**, 262–267 (1992).

[16] Byram, B. and Shu, J., "Pseudononlinear ultrasound simulation approach for reverberation clutter," *Journal of Medical Imaging* **3**(4) (2016).

[17] Byram, B. and Shu, J., "A pseudo non-linear method for fast simulations of ultrasonic reverberation," *Medical Imaging 2016: Ultrasonic Imaging and Tomography* **9790**(April 2016), 1–7 (2016).

[18] Schlunk, S., Dei, K., and Byram, B., "Iterative model-based beamforming for high dynamic range applications," *IEEE Transactions on Ultrasonics, Ferroelectrics, and Frequency Control* , 1–1 (2020).

[19] Lediju, M. A., Pihl, M. J., Dahl, J. J., and Trahey, G. E., "Quantitative assessment of the magnitude, impact and spatial extent of ultrasonic clutter," *Ultrasonic Imaging* **30**(3), 151–168 (2008).

[20] Dei, K., Schlunk, S., Luchies, A., Brown, D., and Byram, B., "Assessment of Tissue Boundary Delineation Using Fundamental and Harmonic ADMIRE and SLSC for Percutaneous Biopsy Guidance," *IEEE International Ultrasonics Symposium, IUS* **2018-Janua**(2), 1–4 (2018).

[21] Luchies, A. C. and Byram, B. C., "Deep Neural Networks for Ultrasound Beamforming," *IEEE Transactions on Medical Imaging* **37**, 2010–2021 (9 2018).